

Lawrence Berkeley National Laboratory

Lawrence Berkeley National Laboratory

Title

The influence of projectile neutron number in the $^{208}\text{Pb}(^{48}\text{Ti}, n)^{255}\text{Rf}$ and $^{208}\text{Pb}(^{50}\text{Ti}, n)^{257}\text{Rf}$ reactions

Permalink

<https://escholarship.org/uc/item/09z839x2>

Author

Dragojevic, I.

Publication Date

2008-09-02

The influence of projectile neutron number in the $^{208}\text{Pb}(^{48}\text{Ti}, n)^{255}\text{Rf}$ and $^{208}\text{Pb}(^{50}\text{Ti}, n)^{257}\text{Rf}$ reactions

I. Dragojević^{1,2}, K.E. Gregorich², Ch. E. Düllmann^{1,2,3}, M.A. Garcia^{1,2}, J.M. Gates^{1,2},
S.L. Nelson^{1,2}, L. Stavsetra², R. Sudowe^{2,*}, and H. Nitsche^{1,2}

¹ Department of Chemistry, University of California, Berkeley, California 94720, U.S.A.

² Nuclear Science Division, Lawrence Berkeley National Laboratory, Berkeley, California 94720, U.S.A.

³ Abteilung Kernchemie, Gesellschaft für Schwerionenforschung mbH, 64291 Darmstadt, Germany

ABSTRACT

Four isotopes of rutherfordium, $^{254-257}\text{Rf}$, were produced by the $^{208}\text{Pb}(^{48}\text{Ti}, xn)^{256-x}\text{Rf}$ and $^{208}\text{Pb}(^{50}\text{Ti}, xn)^{258-x}\text{Rf}$ reactions ($x = 1, 2$) at the Lawrence Berkeley National Laboratory 88-Inch Cyclotron. Excitation functions were measured for the $1n$ and $2n$ exit channels. A maximum likelihood technique, which correctly accounts for the changing cross section at all energies subtended by the targets, was used to fit the $1n$ data to allow a more direct comparison between excitation functions obtained under different experimental conditions. The maximum $1n$ cross sections of the $^{208}\text{Pb}(^{48}\text{Ti}, n)^{255}\text{Rf}$ and $^{208}\text{Pb}(^{50}\text{Ti}, n)^{257}\text{Rf}$ reactions obtained from fits to the experimental data are 0.38 ± 0.07 nb and 40 ± 5 nb, respectively. Excitation functions for the $2n$ exit channel were also measured, with maximum cross sections of $0.40^{+0.27}_{-0.17}$ nb for the ^{48}Ti induced reaction, and 15.7 ± 0.2 nb for the ^{50}Ti induced reaction. The impact of the two neutron difference in the projectile on the $1n$ cross section is discussed. The results are compared to the *Fusion by Diffusion* model developed by Świątecki, Wilczyńska, and Wilczyński.

PACS numbers: 25.70.Gh, 27.90.+b, 23.60.+e

I. INTRODUCTION

When forming nuclides of the heaviest elements in compound nucleus - evaporation reactions between projectiles from ^{48}Ca through ^{70}Zn and targets of ^{208}Pb or ^{209}Bi [1-6], compound nuclei can be formed at excitation energies as low as ~ 12 MeV. Thus this type of reaction has been referred to as “cold fusion.” Cold fusion reactions have been used in the discovery of elements 107-111 [2, 3] and for the synthesis of elements 112 and 113 [1, 4], and are an indispensable tool in the study of heavy element formation and decay [2, 3].

We have studied the influence of the projectile neutron number on the cross section magnitude in the $^{208}\text{Pb}(^{48}\text{Ti}, n)^{255}\text{Rf}$, $^{208}\text{Pb}(^{50}\text{Ti}, n)^{257}\text{Rf}$ reaction pair. The theoretical model that we used as a guide in our cold fusion studies was recently developed by Świątecki *et al.* and is called *Fusion by Diffusion* (FBD) [7, 8]. According to FBD, the cross section is given by:

$$\sigma_{tot} = \sigma_{cap} \cdot P_{CN} \cdot P_{surv}. \quad (1)$$

The cross section is the product of three factors: 1) the probability σ_{cap} for target and projectile nuclei to overcome the Coulomb barrier and become trapped in a pocket of their mutual potential, 2) the probability P_{CN} to proceed from this di-nuclear configuration to form a compound nucleus, and 3) the survival probability P_{surv} , which is the product of

the probability Γ_n/Γ_{tot} to survive a single stage of de-excitation by neutron evaporation in competition with all other de-excitation modes (predominantly fission), and the probability $P_<$ that after evaporation of the neutron, the excitation energy is less than the threshold for second neutron emission or second chance fission.

A neutron evaporation spectrum is a Boltzmann distribution of the form $E_{kin} \cdot \exp(-E_{kin}/T)$, where E_{kin} is the kinetic energy of the evaporation neutron, and T is the transition state temperature for the neutron emission. Since $P_<$ is essentially a neutron evaporation spectrum integrated over an energy range from K to infinity, where $K = E - E_{th}$, and E_{th} is the second chance fission threshold, $P_<$ is then given by:

$$P_< = (1 + \frac{K}{T}) \cdot \exp(-\frac{K}{T}) \quad \text{if } K \geq 0, \quad (2)$$

$$P_< = 1 \quad \text{if } K \leq 0. \quad (3)$$

While equation (1) may be an old formulation, it is the one used by many theorists modeling heavy element formation by compound nucleus reactions today [7-14]. The FBD model treats the probability to form the compound nucleus, P_{CN} , as a statistical diffusion across a coordinate corresponding to the overall length of the di-nuclear system. This FBD model was shown to reproduce experimental maximum cross sections of reactions leading to evaporation residues spanning a broad range in Z to within a factor of 2 [7, 8]. In addition to the predicted heights of the excitation functions, it provides us with other testable predictions, such as the location of excitation function maxima [6, 15, 16], shapes of excitation functions, and cross section ratios between reaction pairs (for example, reaction pairs where the target stays the same, but projectiles differ by two neutrons, or reaction pairs with two different projectile-target combinations that lead to a

formation of the same compound nucleus). Recent theoretical predictions by Świątecki *et al.* indicate surprisingly large differences in cross sections for cold fusion reactions between reaction pairs differing by two neutrons in the projectile [17]. To test this aspect of the model, we studied the $^{208}\text{Pb}(^{48}\text{Ti}, n)^{255}\text{Rf}$ and $^{208}\text{Pb}(^{50}\text{Ti}, n)^{257}\text{Rf}$ fusion reactions. This reaction pair is of particular interest because the predicted maximum cross section for the $^{208}\text{Pb}(^{50}\text{Ti}, n)^{257}\text{Rf}$ reaction is ~ 37 times larger than the maximum predicted cross section for the $^{208}\text{Pb}(^{48}\text{Ti}, n)^{255}\text{Rf}$ reaction. The two excitation functions are also predicted to have different shapes. While a complete excitation function for the ^{50}Ti -induced reaction has been previously reported in [18, 19], the $^{208}\text{Pb}(^{48}\text{Ti}, n)^{255}\text{Rf}$ excitation function is presented for the first time in this work.

II. EXPERIMENTAL TECHNIQUE

A. Production of $^{256,257}\text{Rf}$ via the $^{50}\text{Ti} + ^{208}\text{Pb}$ Reaction

The Lawrence Berkeley National Laboratory (LBNL) Advanced Electron Cyclotron Resonance source (AECR-U) [20] was used to produce ^{50}Ti ions in the 12+ charge state. The ions were then accelerated by the LBNL's 88-Inch Cyclotron to energies ranging from 4.6-4.8 MeV/nucleon. The beam passed through a $45 \mu\text{g}/\text{cm}^2$ carbon window separating the beamline vacuum from the 66 Pa helium gas inside the Berkeley Gas-filled Separator (BGS) [21-23], and then through the ^{208}Pb targets (98.4% ^{208}Pb , 1.1% ^{207}Pb , and 0.5% ^{206}Pb). We conducted two separate experiments, one with thick ($470 \mu\text{g}/\text{cm}^2$) and one with thin ($104 \mu\text{g}/\text{cm}^2$) ^{208}Pb targets. The thin ^{208}Pb targets, evaporated on $38 \mu\text{g}/\text{cm}^2$ carbon backings, were used for the $1n$ excitation function measurement at five distinct lab-frame center-of-target energies: 228.5, 229.5, 230.5, 232.6, and 234.6 MeV.

The energy loss in the ^{208}Pb layer was approximately 1 MeV [24, 25]. In a separate experiment, we used the thick ^{208}Pb targets, evaporated on $45 \mu\text{g}/\text{cm}^2$ carbon backings, to measure the $1n$ and $2n$ cross sections at three additional lab-frame center-of-target energies: 236.0, 239.0, and 242.0 MeV. The energy loss in the thick ^{208}Pb targets was approximately 4.2 MeV. Excitation energies corresponding to these center-of-target energies were calculated by using experimental mass defects [26] for projectile and target masses, and Thomas-Fermi mass defects [27] for the compound nucleus (CN) masses. The excitation energies subtended by the target were 14.7 ± 0.4 , 15.5 ± 0.4 , 16.3 ± 0.4 , 17.9 ± 0.4 , 19.5 ± 0.4 , 21.3 ± 2.1 , 23.3 ± 2.1 , and 25.6 ± 2.1 MeV. The targets were mounted on the perimeter of a rotating wheel (35.6 cm in diameter) located 1 cm downstream from the carbon window. To increase radiative target cooling, a $10 \mu\text{g}/\text{cm}^2$ layer of carbon was evaporated onto the downstream side of the targets. The wheel was rotated at approximately 8.5 Hz to minimize beam-induced target heating. To measure the product of the beam intensity and target thickness, two silicon $p-i-n$ detectors were mounted at an azimuthal angle of 27° relative to the beam axis to measure the Rutherford-scattered projectiles. The pulse height of the Rutherford-scattered projectiles was used to determine the relative beam energies with high accuracy. The systematic error in the absolute beam energies from the cyclotron is 1%, while the error in determining the relative energies is less than 0.08%. The beam intensities ranged from 0.17-0.4 particle- μA . After recoiling out of the target, rutherfordium evaporation residues (EVRs) were separated from other reaction products based on their differing magnetic rigidities in helium gas. Magnetic rigidities have been estimated by using a semi-empirical formula [22]. The detection setup for the experiment with the thin targets was slightly different

from the detection setup employed for the experiment with the thick targets. In the experiment with the thin ^{208}Pb targets, a focal plane detector was used to detect the recoils. The focal plane detector consisted of three silicon cards (each $6 \times 6 \text{ cm}^2$), each consisting of 16 vertical strips, giving a total of 48 silicon strips which provide horizontal resolution. The vertical position was determined by resistive charge division, from the charges collected at the top and the bottom of each strip. Eight additional silicon cards, each with 4 sets of 4 strips galvanically connected, were mounted perpendicular to the focal plane detector giving the total of 32 signals. This non-position-sensitive “upstream” detector together with the focal plane detector made a five-sided box configuration. This configuration provides additional detection efficiency for α -particles or fission fragments emitted from the species implanted in the surface of the focal plane detector. When an α -particle or fission fragments are detected both in the focal plane detector and in the upstream detector, the total energy is then the sum of focal plane and upstream energies. In the search for decay chains, these “reconstructed” events were treated the same as if they had deposited full energy in the focal plane detector. We also considered two additional types of events in the search for the decay chains: 1) escapes (esc), events in which an α -particle “escapes” from the surface of the focal plane detector and leaves only a partial signal in it (typically 0.5-5 MeV), and 2) missing alphas (miss α), events in which an alpha is not detected and is missing from the chain. A “punch-through” veto detector, consisting of 3 silicon cards, (also each with 4 sets of 4 strips joined together, resulting in a total of 12 electronic channels), was mounted directly behind the focal plane detector. Any signal in the punch-through detector, typically coming from light and low-ionizing particles passing through the focal plane detector

chips, was used to veto any other coincident signals coming from other detectors in the offline analysis. A multi-wire proportional counter (MWPC) was placed upstream from the focal plane detector. The presence or absence of signals from the MWPC in coincidence with signals from the focal plane detector allowed for discrimination between implantation events and radioactive decays in the focal plane detector. The α -particle energy resolution in the focal plane detector was 55 keV FWHM, and approximately 100 keV for the reconstructed α -particle energies. The vertical position resolution within a single strip can be approximated by $\sigma_y(E) = 2800 \text{ keV/mm}$. Details of our detection system have also been described previously in [6, 28].

The experiment involving the thick targets had a similar experimental setup except that a double sided silicon strip detector (DSSD) was used instead, and there were no upstream or punch-through detectors. The DSSD is 1 mm thick has 16 horizontal and 16 vertical strips ($5 \times 5 \text{ cm}^2$), allowing for a very good position (the pixel size is $\sim 3 \text{ mm}^2$) and energy resolution (35 keV).

The identification of ^{257}Rf was based on the observation of an EVR ($8.0 < E \text{ (MeV)} < 20.0$, prompt time-of-flight (TOF) signal between the focal plane and the MWPC, no punch-through signal, no upstream signal) followed by a ^{257}Rf alpha particle ($8.0 < E \text{ (MeV)} < 9.3$, no MWPC signal, no punch through signal) within 25 s (see Fig. 1 for decay properties as given in [29]) from the same vertical position of the same detector strip (or in the same pixel when the DSSD was used). The rate of “EVR-like events” was 1.55 Hz when the focal plane detector was used. The rate of “ ^{257}Rf -like events” was 0.045 Hz. Under these conditions, the random rate calculation (performed as described in [16]) indicates that out of 139 chains observed with the thin targets, less than 0.9

chains result from random correlation of unrelated events. For the three highest energies, (where the DSSD was used), the rate of “EVR-like events” was 0.18 Hz, and the rate of “ ^{257}Rf -like events” was 9.7×10^{-2} Hz. Out of 203 chains observed in the experiment with the thick targets, 0.3 chains of random origin are expected. The BGS efficiency, eff (the fraction of all Rf EVRs that are implanted into the silicon strip detector), for this reaction has been estimated by means of a Monte Carlo simulation [22, 23], which resulted in $eff = 0.76 \pm 0.08$ (when the thin targets were used with the larger focal plane detector), or $eff = 0.40 \pm 0.05$ (when the thick targets were used with the smaller DSSD). The efficiencies for detecting ^{257}Rf alpha particles were 0.68 (in the focal plane only or reconstructed events with both focal plane and an upstream signal) and 0.50 in the DSSD.

The $^{208}\text{Pb}(^{50}\text{Ti}, 2n)^{256}\text{Rf}$ excitation function was measured under experimental conditions that were identical to the ones described above for the $^{208}\text{Pb}(^{50}\text{Ti}, 1n)^{257}\text{Rf}$ reaction with the thick targets and the DSSD. ^{256}Rf atoms were identified by observation of an EVR ($8.0 < E \text{ (MeV)} < 20.0$, TOF signal between the DSSD and the MWPC) followed by a spontaneous fission ($E \text{ (MeV)} > 90$ MeV, no TOF signal between the DSSD and the MWPC) within 150 ms in the same DSSD pixel. The rate of the “EVR-like” events in the DSSD was 0.18 Hz and the rate of “ ^{256}Rf -like” events was 7.0×10^{-3} Hz. Out of 5259 observed chains, 0.2 may result from random correlations.

B. Production of $^{254,255}\text{Rf}$ via the $^{48}\text{Ti} + ^{208}\text{Pb}$ Reaction

The experimental set-up for $^{208}\text{Pb}(^{48}\text{Ti}, n)^{255}\text{Rf}$ reaction was very similar to the previously described ^{257}Rf setup (with the focal plane, upstream, and punch-through

detectors). Thin ($104 \mu\text{g}/\text{cm}^2$) and thick targets ($470 \mu\text{g}/\text{cm}^2$) were used to produce ^{255}Rf . To obtain a statistically significant result within a relatively short irradiation time, thick lead targets were used to measure the high energy side of the excitation function. This, however, resulted in reduced excitation function energy resolution. ^{255}Rf was identified by observing an “EVR-like event” ($8.0 < E \text{ (MeV)} < 20.0$, prompt TOF signal between the focal plane and the MWPC, no punch through signal, no upstream signal) followed by a spontaneous fission ($E \text{ (MeV)} > 90$, no TOF signal between the focal plane and the MWPC), or an “EVR-like event” followed by an “ ^{255}Rf -like event” ($8.0 < E \text{ (MeV)} < 10.0$, no MWPC signal, no punch through signal) within 10 s, and then by a ^{251}No and/or ^{247}Fm daughter ($7.5 < E \text{ (MeV)} < 9.5$, no MWPC signal, no punch through signal) within 175 s. To minimize the contribution from randomly correlated unrelated events, a fast beam-shutoff was employed whenever an EVR was detected and followed by a “Rf-like event”. The beam was switched off for 140 s, allowing us to observe possible decays of the nobelium or fermium daughters in a low background environment. The calculated number of random EVR- α - α correlations of 8×10^{-4} shows an insignificant contribution from random correlations. The expected contribution of EVR-SF randomly correlated unrelated events is 0.6.

While the BGS efficiency for this reaction was the same as for the ^{257}Rf reaction, the efficiency for detection of ^{255}Rf chains (total efficiency for observing either one of the following cases: 1) EVR-SF, 2) EVR- α_1 - α_2 , 3) EVR-esc- α_2 or EVR- α_1 -esc, and 4) EVR-miss α_1 - α_2 - α_3) was 0.91. Here α_1 , α_2 , and α_3 , correspond to alphas of ^{255}Rf , ^{251}No , and ^{247}Fm , respectively. An event is considered a valid escape only if it occurs in the same position (same strip and with the vertical position within $\pm 1.5 \text{ mm}$) as the rest of

the chain, and if its lifetime is consistent with the half-life of the isotope we expected at that position within a chain. Only ^{255}Rf or ^{251}No escapes were considered, while the potential ^{247}Fm escapes were neglected due to the long half-life and increased possibility of random correlations.

The $^{208}\text{Pb}(^{48}\text{Ti}, 2n)^{254}\text{Rf}$ excitation function was also measured in the same experiment. ^{254}Rf atoms were identified by observation of an EVR as defined above, followed by a spontaneous fission in the same pixel within 120 μs . The rate of “EVR-like” events was 0.58 Hz, the rate of “ ^{254}Rf -like” events was 5.6×10^{-5} Hz, and the number of expected chains resulting from random correlations was 7×10^{-7} .

III. RESULTS AND DISCUSSION

Table I shows a summary of the experimental conditions, the number of events observed at the individual energies, and the measured cross sections for both $^{208}\text{Pb}(^{50}\text{Ti}, xn)^{258-xn}\text{Rf}$ and $^{208}\text{Pb}(^{48}\text{Ti}, xn)^{256-xn}\text{Rf}$ reactions.

A. $^{208}\text{Pb}(^{50}\text{Ti}, 1n)^{257}\text{Rf}$ and $^{208}\text{Pb}(^{50}\text{Ti}, 2n)^{256}\text{Rf}$ Excitation functions

The $^{208}\text{Pb}(^{50}\text{Ti}, n)^{257}\text{Rf}$ excitation function is shown in the upper portion of Fig. 2. The figure shows the data along with a fit using the maximum likelihood technique as described in the Appendix. The prediction of the *Fusion by Diffusion* model and the data from Ref. [18] are also shown in the figure. The centroid value of the fit, c' , which represents the excitation energy at which the maximum cross section is located, is 16.6 MeV. This is 2.2 MeV larger than 14.4 MeV predicted by the FBD. The peak cross

section in the fit is 40 ± 5 nb, which is significantly larger than the previously reported value of 15 nb [18] and the FBD prediction of 26 nb. Applying our fitting procedure to the data in Ref. [18] to remove the target thickness factor in determining the height of the excitation function, resulted in a cross section of ~ 21.5 nb, which is still nearly a factor of two lower than measured in this work. The smaller value reported in Ref. [18] is presumably the average cross section over a 4 MeV target. The excitation function measured in this work has a slightly asymmetric shape. This asymmetry was not observed in [18] because the old fits used the average cross section at each point, rather than integrated cross section over the target energy thickness, the method used in this work. We have observed a total of 242 ^{257}Rf events. The observed α -decay energies were between 8300-9150 keV, and they were assigned either to ^{257}Rf or its electron capture (EC) daughter, ^{257}Lr . A detailed half-life and α -decay analysis indicates the presence of two distinct states in ^{257}Rf , one with alpha energies in the 8300 - 8800 keV range ($T_{1/2} = 7.2^{+1.3}_{-1.1}$ s) and the other one in the 8900 - 9150 keV range ($T_{1/2} = 4.1^{+0.7}_{-0.6}$ s). Hessberger *et al.* assigned events with $8200 < E_{\alpha} < 8800$ keV to the ground state and events with $E_{\alpha} > 8900$ keV to the isomer. These assignments are based on the comparison between the ^{257}Rf decay data obtained from the direct production of ^{257}Rf in $^{208}\text{Pb}(^{50}\text{Ti}, n)^{257}\text{Rf}$ reaction in which α -decays in the region $E_{\alpha} = (8200-9100)$ keV were observed, and ^{257}Rf decay data obtained via α -decay of ^{265}Hs (from the $^{58}\text{Fe} + ^{208}\text{Pb}$ reaction [30]), in which essentially all ^{257}Rf events were found at $E_{\alpha} < 8800$ keV [31]. This argument is based on the assumption that in the $^{265}\text{Hs} \rightarrow ^{261}\text{Sg} \rightarrow ^{257}\text{Rf}$ chain, ^{261}Sg decays predominantly to the ground state of ^{257}Rf . However, without α - γ decay studies to acquire more knowledge about the ^{257}Rf level scheme, it is impossible to determine

which state is the isomer and which is the ground state, and whether additional isomeric states exist. The total branching ratio for the EC decay

$$\left(\frac{N_{\alpha}(^{257}\text{Lr})}{N_{\alpha}(^{257}\text{Lr}) + N_{\alpha}(^{257}\text{Rf}^a) + N_{\alpha}(^{257}\text{Rf}^b)} \right),$$

where N_{α} is the number of alphas observed, and a and b denote the two isomers of ^{257}Rf of ^{257}Rf is 14 ± 1 %. The present data are insufficient to distinguish between EC decays of the two isomers. The half-life of the ^{257}Rf state belonging to the higher alpha energy group is in agreement with the literature value, but the half-life of the state belonging to the lower alpha energy group is longer than the literature value by almost a factor of two [19, 29].

In a separate experiment, we have also measured the $^{208}\text{Pb}(^{50}\text{Ti}, 2n)^{256}\text{Rf}$ excitation function, which is shown in Fig. 3. The ^{256}Rf half-life measured in this experiment is 6.70 ± 0.09 ms, which is in a good agreement with $T_{1/2} = 7.4_{-0.7}^{+0.9}$ ms from Ref. [32] and slightly larger than the $T_{1/2} = 6.2 \pm 0.2$ ms from Ref. [19]. The measured peak cross section for the $2n$ exit channel is 15.8 ± 0.2 nb, which agrees with the one from Ref. [18]. The centroid is located at 23.3 MeV, compared to 21.1 MeV for the $2n$ data from Ref. [18].

B. $^{208}\text{Pb}(^{48}\text{Ti}, n)^{255}\text{Rf}$ and $^{208}\text{Pb}(^{48}\text{Ti}, 2n)^{254}\text{Rf}$ Excitation Functions

An integrated cross section for the $^{208}\text{Pb}(^{48}\text{Ti}, n)^{255}\text{Rf}$ reaction over a wide energy range (from the threshold up to a maximum laboratory frame energy of 5.40 MeV/nucleon) was measured earlier by Oganessian *et al.*, and is reported to be 0.2 nb [33]. An upper limit for the $2n$ cross section of 1 nb was reported in Ref. [34]. In our

study the full $^{208}\text{Pb}(^{48}\text{Ti}, n)^{255}\text{Rf}$ and $^{208}\text{Pb}(^{48}\text{Ti}, 2n)^{254}\text{Rf}$ excitation functions were measured for the first time. The excitation functions are shown in Figures 2 and 3. The measured half-life of ^{255}Rf is $1.6_{-0.2}^{+0.3}$ s, which is in good agreement with the literature value [29, 31]. A maximum likelihood fit to our $1n$ excitation function results in a maximum cross section of 0.38 ± 0.07 nb, lower than the FBD prediction of 0.68 nb. The FBD also predicts the peak at an excitation energy of 15.5 MeV, 1.3 MeV lower than the centroid value from the fit, $c' = 16.8$ MeV. This suggests that the cross section is heavily influenced by the location of the barrier, which is at an excitation energy about 9 MeV higher than the centroid of the $1n$ excitation function. Because the cross section is dominated by the Coulomb term, σ_{cap} , small errors in the barrier position can easily lead to relatively pronounced differences between predicted and measured cross sections.

Figure 4 shows a plot of σ_{cap} as a function of the lab-frame energy. The second chance fission thresholds for the $^{48}\text{Ti} + ^{208}\text{Pb}$ and $^{50}\text{Ti} + ^{208}\text{Pb}$ reactions are 218.3 and 225.6 MeV, respectively [26, 27]. The σ_{cap} value at the second chance fission threshold energy is 1.78 mb for the $^{50}\text{Ti} + ^{208}\text{Pb}$ reaction and 0.035 mb for $^{48}\text{Ti} + ^{208}\text{Pb}$ reaction. The ratio of the experimental cross sections for the $^{208}\text{Pb}(^{50}\text{Ti}, n)^{257}\text{Rf}$ and $^{208}\text{Pb}(^{48}\text{Ti}, n)^{255}\text{Rf}$ reactions is 101_{-22}^{+34} , while the ratio of the corresponding σ_{cap} cross sections is 50.9.

Therefore, the difference in σ_{cap} accounts for much of the difference between the two experimental $1n$ cross sections for these reactions. This demonstrates that the correct parameterization of the barrier, which is a part of the fusion probability equation, is essential to correctly predicting the magnitude of the excitation function maximum.

We have also measured the $^{208}\text{Pb}(^{48}\text{Ti}, 2n)^{254}\text{Rf}$ excitation function at higher excitation energies with a cross section maximum of 0.31 ± 0.8 nb, corrected for the

events lost due to the dead time of the data acquisition system (13 μ s). The centroid is located at $E^* = 21.5$ MeV. The $2n$ excitation function is shown in Fig. 3. The cross section summary for both reactions is given in Table 1. The ^{254}Rf half-life was measured as $29.6_{-0.6}^{+0.7}$ μ s, which is slightly higher than the previously reported value of 23 ± 3 μ s from Ref. [19].

IV. CONCLUSION

We have measured the $1n$ and $2n$ excitation functions for the $^{48}\text{Ti} + ^{208}\text{Pb}$ and $^{50}\text{Ti} + ^{208}\text{Pb}$ reactions. The experimental ratio of the $^{208}\text{Pb}(^{50}\text{Ti}, n)^{257}\text{Rf}$ and $^{208}\text{Pb}(^{48}\text{Ti}, n)^{255}\text{Rf}$ cross sections is 101_{-22}^{+34} . The experimental maximum cross section of the $^{208}\text{Pb}(^{48}\text{Ti}, n)^{255}\text{Rf}$ excitation function is a factor of $1.8_{-0.3}^{+0.4}$ smaller than the FBD prediction, and the centroid is located at an excitation energy 1.3 MeV higher than the FBD prediction. For the $^{208}\text{Pb}(^{50}\text{Ti}, n)^{257}\text{Rf}$ excitation function the experimental cross section is 1.6 ± 0.2 times larger than the FBD prediction. Table II shows the comparison between the experimental data and the FBD theoretical model. The difference in shape between the $^{208}\text{Pb}(^{50}\text{Ti}, n)^{257}\text{Rf}$ and $^{208}\text{Pb}(^{48}\text{Ti}, n)^{255}\text{Rf}$ excitation functions follows the predicted trend, although the difference is more pronounced than predicted by the FBD model. The plot of FBD predictions along with the experimental data is shown in Figure 2. While FBD and other theoretical models do an admirable job reproducing the experimental excitation functions, our high resolution data can be used to refine and improve these models.

ACKNOWLEDGEMENTS

We would like to thank the operations and the ECR ion source staff of the 88-Inch Cyclotron for help and support during the experiment. The authors also wish to thank W. J. Świątecki for his predictions and helpful discussions, and the staff of the GSI target lab for providing some of the targets used in these experiments.

This work was supported by the Director, Office of Science, Office of Basic Energy Sciences, of the U.S. Department of Energy under Contract No. DE-AC02-05CH11231.

APPENDIX : FITTING METHODS

Excitation function fits were obtained with a maximum likelihood technique [35-38]. Inspection of various cold fusion excitation functions reveals that their shape resembles a Gaussian on the lower energy side with an exponentially decreasing tail on the high energy side. To fit our data, we used a function that consisted of a Gaussian on the low-energy side smoothly joined to an exponential on the high-energy side.

$$\sigma = \sigma_{\max} e^{-(E_{COT}^* - c)^2 / 2w^2}, \quad E_{COT}^* \leq \lambda w^2 + c \quad (A1)$$

$$\sigma = \sigma_{\max} e^{\lambda^2 w^2 / 2} e^{-\lambda(E_{COT}^* - c)}, \quad E_{COT}^* > \lambda w^2 + c$$

Here E_{COT}^* is the excitation energy, σ_{\max} represents the amplitude of a Gaussian with a centroid c and width w . The exponential slope is $-\lambda$. For each beam energy, the number of counts expected, μ , is calculated by integrating σ over the energy width of the target,

$$\mu_{\text{expected}}(L, E_{COT}^*, E_w, \sigma_{\max}, w, c, \lambda) = \frac{L}{E_w} \int_{E_{COT}^* - \frac{E_w}{2}}^{E_{COT}^* + \frac{E_w}{2}} \sigma(\sigma_{\max}, w, c, \lambda, E) dE \quad (A2)$$

where L represents one event sensitivities in events/pb, E_{COT}^* is the excitation energy at the center of target, and E_w is the energy width of the target. At each beam energy, we used the Poisson distribution to calculate the probability of observing n events where μ are expected. The relative likelihood, L , that the fit represents the excitation function data is the product of the Poisson probabilities at each of m energies, is given by:

$$L(\sigma_{\max}, w, c, \lambda) = \prod_{i=1}^m \frac{\mu^{n_i}}{n_i!} \cdot e^{-\mu}.$$

(A3)

The expression obtained is then maximized to obtain the best fitting parameters σ' , w' , c' , and λ' . The fitting curve is obtained from:

$$f(\sigma', w', c', \lambda') = \frac{\mu}{L} \tag{A4}$$

The fit parameters for both ^{48}Ti and ^{50}Ti reactions, are listed in Table II. This fitting method is more appropriate than other simpler fitting techniques because it integrates the excitation function over the energy width of the target and it takes into account the statistical significance of each point. Moreover, this fitting technique allows for an easier comparison between excitation functions measured at different laboratories and with different target thicknesses.

*Present address: Department of Health Physics, University of Nevada, Las Vegas, Las Vegas, NV 89154, USA

[1] S. Hofmann, *et al.*, Eur. Phys. J. A **14**, 147 (2002).

- [2] S. Hofmann and G. Münzenberg, *Rev. Mod. Phys.* **72**, 733 (2000).
- [3] S. Hofmann, *Rep. Prog. Phys.* **61**, 639 (1998).
- [4] K. Morita, Morimoto, K., et al., *J. Phys. Soc. of Jpn.* **76**, 043201 (2007).
- [5] K. Morita, *et al.*, *Eur. Phys. J. A* **21**, 257 (2004).
- [6] C. M. Folden III, K. E. Gregorich, Ch. E. Düllmann, H. Mahmud, G. K. Pang, J. M. Schwantes, R. Sudowe, P. M. Zielinski, H. Nitsche, and D. C. Hoffman, *Phys. Rev. Lett.* **93**, 212702 (2004).
- [7] W. J. Świątecki, K. Siwek-Wilczyńska, and J. Wilczyński, *Acta. Phys. Pol. B* **34**, 2049 (2003).
- [8] W. J. Świątecki, K. Siwek-Wilczyńska, and J. Wilczyński, *Phys. Rev. C* **71**, 014602 (2005).
- [9] V. I. Zagrebaev, M. G. Itkis, and Y. T. Oganessian, *Phys. Atom. Nucl.* **66**, 1033 (2003).
- [10] G. G. Adamian, N. V. Antonenko, R. V. Jolos, Y. V. Palchikov, W. Scheid, and T. A. Shneidman, *Phys. Atom. Nucl.* **67**, 1701 (2004).
- [11] G. G. Adamian, N. V. Antonenko, and W. Scheid, *Phys. Rev. C* **69**, 044601 (2004).
- [12] Z. Q. Feng, G. M. Jin, J. Q. Li, and W. Scheid, *Phys. Rev. C* **76**, 044606 (2007).
- [13] Z. Q. Feng, G. M. Jin, F. Fu, and J. Q. Li, *Nucl. Phys.* **A771**, 50 (2006).
- [14] Y. Aritomo, *Phys. Rev. C* **75**, 024602 (2007).
- [15] S. L. Nelson, K. E. Gregorich, I. Dragojević, M. A. Garcia, J. M. Gates, R. Sudowe, and H. Nitsche, *Phys. Rev. Lett.* **100**, 022501 (2008).

- [16] C. M. Folden III, S. L. Nelson, Ch. E. Düllmann, J. M. Schwantes, R. Sudowe, P. M. Zielinski, K. E. Gregorich, H. Nitsche, and D. C. Hoffman, *Phys. Rev. C* **73**, 014611 (2006).
- [17] W. J. Świątecki, (private communication, 2007.)
- [18] S. Hofmann, *et al.*, *Nucl. Phys.* **A734**, 93 (2004).
- [19] F. P. Hessberger, *et al.*, *Z. Phys. A* **359**, 415 (1997).
- [20] X. Zu Qi and C. M. Lyneis, *Rev. Sci. Instrum.* **67**, 886 (1996).
- [21] W. Loveland, K. E. Gregorich, J. B. Patin, D. Peterson, C. Rouki, P. M. Zielinski, and K. Aleklett, *Phys. Rev. C* **66**, 044617 (2002).
- [22] K. E. Gregorich, *et al.*, *Phys. Rev. C* **72**, 014605 (2005).
- [23] K. E. Gregorich, *et al.*, *Eur. Phys. J. A* **18**, 633 (2003).
- [24] J. F. Ziegler, *Nucl. Instrum. Methods B* **219-20**, 1027 (2004).
- [25] J. F. Ziegler, computer software SRIM-2006, available from <http://www.srim.org/SRIM/SRIM2006.htm>.
- [26] G. Audi, A. H. Wapstra, and C. Thibault, *Nucl. Phys.* **A729**, 337 (2003).
- [27] W. D. Myers and W. J. Świątecki, LBL-36803 (1994).
- [28] K. E. Gregorich, *et al.*, *Phys. Rev. C* **74**, 044611 (2006).
- [29] F. P. Hessberger, *et al.*, *Eur. Phys. J. A* **12**, 57 (2001).
- [30] S. Hofmann, F. P. Hessberger, V. Ninov, P. Armbruster, G. Münzenberg, C. Stodel, A. G. Popeko, A. V. Yeremin, S. Saro, and M. Leino, *Z. Phys. A* **358**, 377 (1997).
- [31] F. P. Hessberger, *et al.*, *Z. Phys. A* **359**, 415 (1997).

- [32] F. P. Hessberger, G. Münzenberg, S. Hofmann, W. Reisdorf, K. H. Schmidt, H. J. Schött, P. Armbruster, R. Hingmann, B. Thuma, and D. Vermeulen, *Z. Phys. A* **321**, 317 (1985).
- [33] Y. T. Oganessian, *et al.*, *Radiochim. Acta* **37**, 113 (1984).
- [34] G. M. Ter-Akopyan, A. S. Iljinov, Y. T. Oganessian, O. A. Orlova, G. S. Popeko, S. P. Tretyakova, V. I. Chepigin, B. V. Shilov, and G. N. Flerov, *Nucl. Phys.* **A255**, 509 (1975).
- [35] R. A. Fisher, *Proc. R. Soc. A* **144**, 0285 (1934).
- [36] R. A. Fisher, *Proc. R. Soc. A* **146**, 0001 (1934).
- [37] R. A. Fisher, *Proc. Cambridge Philos. Soc.* **28**, 257 (1932).
- [38] R. A. Fisher, *Philos. Trans. R. Soc. London A* **222**, 309 (1922).

Table I: Summary of experimental conditions and results.

E_{LAB}	E_{COT}^*	Σ events	σ_{1n}	Σ events	σ_{2n}
(MeV)	(MeV)	(1n)	(nb)	(2n)	(nb)
$^{208}\text{Pb}(^{48}\text{Ti},x\text{n})^{256-x}\text{Rf}$					
218.8 ^a	12.5	0	0.036 ^c	0	< 0.049 ^c
220.7 ^b	14.8	7	0.11 ^{+0.06} _{-0.04}	0	< 0.038 ^c
222.2 ^b	16.0	7	0.20 ^{+0.11} _{-0.07}	0	<0.072 ^c

223.3 ^b	16.9	12	0.41 ^{+0.16} _{-0.12}	0	<0.063 ^c
223.8 ^a	17.4	10	0.39 ^{+0.17} _{-0.12}	0	<0.098 ^c
225.8 ^b	19.0	5	0.13 ^{+0.08} _{-0.05}	1	0.034 ^{+0.079} _{-0.028}
228.4 ^a	21.1	4	0.23 ^{+0.18} _{-0.11}	5	0.40 ^{+0.27} _{-0.17}
228.8 ^b	21.4	6	0.13 ^{+0.08} _{-0.05}	6	0.17 ^{+0.1} _{-0.07}
233.8 ^a	25.5	1	0.028 ^{+0.064} _{-0.023}	8	0.31 ^{+0.15} _{-0.11}
238.8 ^a	29.5	2	0.049 ^{+0.065} _{-0.032}	4	0.14 ^{+0.11} _{-0.06}
<hr/>					
²⁰⁸ Pb(⁵⁰ Ti, <i>xn</i>) ^{258-x} Rf					
228.5 ^b	14.7	19	11.7 ^{+3.3} _{-2.6}	0	<0.78 ^c
229.5 ^b	15.5	40	26.5 ^{+4.9} _{-4.2}	0	<0.83 ^c
230.5 ^b	16.3	27	43 ⁺¹⁰ ₋₈	1	1.07 ^{+2.5} _{-0.9}
232.6 ^b	17.9	26	20 ⁺⁵ ₋₄	2	1.07 ^{+1.4} _{-0.7}
234.6 ^b	19.5	27	14 ± 3	21	7.5 ^{+2.0} _{-1.6}
236.0 ^b	21.3	61	4.7 ^{+0.7} _{-0.6}	272	9.2 ± 0.6

239.0 ^b	23.3	141	1.0 ± 0.1	4908	15.7 ± 0.2
242.0 ^b	25.6	2	0.38 ^{+0.50} _{-0.24}	79	6.8 ± 0.8

^a Targets were 470 μg/cm² on 40 μg/cm² C.

^b Targets were 104 μg/cm² on 38 μg/cm² C.

^c Upper limit (84% confidence level)

Table II. Comparison between the experimental data and the predictions of the *Fusion by Diffusion* model. Experimental data from reference [18] is also shown for the ⁵⁰Ti+²⁰⁸Pb reaction. SCF and TCF denote the second and third chance fission, respectively.

	²⁰⁸ Pb(⁴⁸ Ti,xn) ²⁵⁵ Rf	²⁰⁸ Pb(⁵⁰ Ti,xn) ²⁵⁷ Rf
<i>E*</i> (1 <i>n</i> , threshold, MeV)	8.24	7.60
<i>E*</i> (Barrier, MeV)	26.0	20.0
<i>E*</i> (2 <i>n</i> , threshold, MeV)	15.2	13.1
<i>E*</i> (SCF threshold)	13.0	12.3
<i>E*</i> (TCF threshold)	19.3	17.8

	Exp. (LBNL)	FBD	Exp. (LBNL)	Exp. (GSI)	FBD
c' (MeV)	16.8 ± 0.2	15.5	16.6 ± 0.1	15.4 ± 0.1	14.4
σ' (nb)	0.38 ± 0.07	0.68	40 ± 2	15 ± 1.9	25.2
λ'	0.18 ± 0.04	0.28	0.52 ± 0.01	0.40 ± 0.02	0.47
w' (MeV)	1.35 ± 0.17	1.18	1.44 ± 0.09	1.32 ± 0.07	1.19

FIG. 1 (Color online) Decay properties of $^{254-257}\text{Rf}$ isotopes and their daughter nuclides. The half-lives for ^{256}Rf and ^{257}Rf are from this work, and the properties of the other nuclei are as reported in Ref. [29].

FIG 2. (Color online) Comparison of the $^{208}\text{Pb}(^{50}\text{Ti}, n)^{257}\text{Rf}$ and $^{208}\text{Pb}(^{48}\text{Ti}, n)^{255}\text{Rf}$ excitation functions. The data from reference [18] are also plotted for a comparison. The dotted lines are the FBD predictions. The arrows indicate the location of the fusion barrier, calculated as in Ref. [8].

FIG. 3. (Color online) Experimental $1n$ and $2n$ excitation functions for $^{50}\text{Ti} + ^{208}\text{Pb}$ (a) and $^{48}\text{Ti} + ^{208}\text{Pb}$ (b). The lines through the $1n$ points are fits to the data as described in the text, while the lines through the $2n$ points are just to guide the eye. Vertical error bars in the $^{208}\text{Pb}(^{50}\text{Ti}, 2n)^{256}\text{Rf}$ excitation function are smaller than the size of the symbols.

Black arrows indicate the threshold energies for the second and third chance fission, calculated from the fission barriers from Ref. [27].

FIG 4. Predicted capture cross section (σ_{cap}) as a function of the lab-frame beam energy.

The black arrows indicate the second chance fission threshold energies for the $^{208}\text{Pb}(^{48}\text{Ti}, n)^{255}\text{Rf}$ and $^{208}\text{Pb}(^{50}\text{Ti}, n)^{257}\text{Rf}$ reactions.

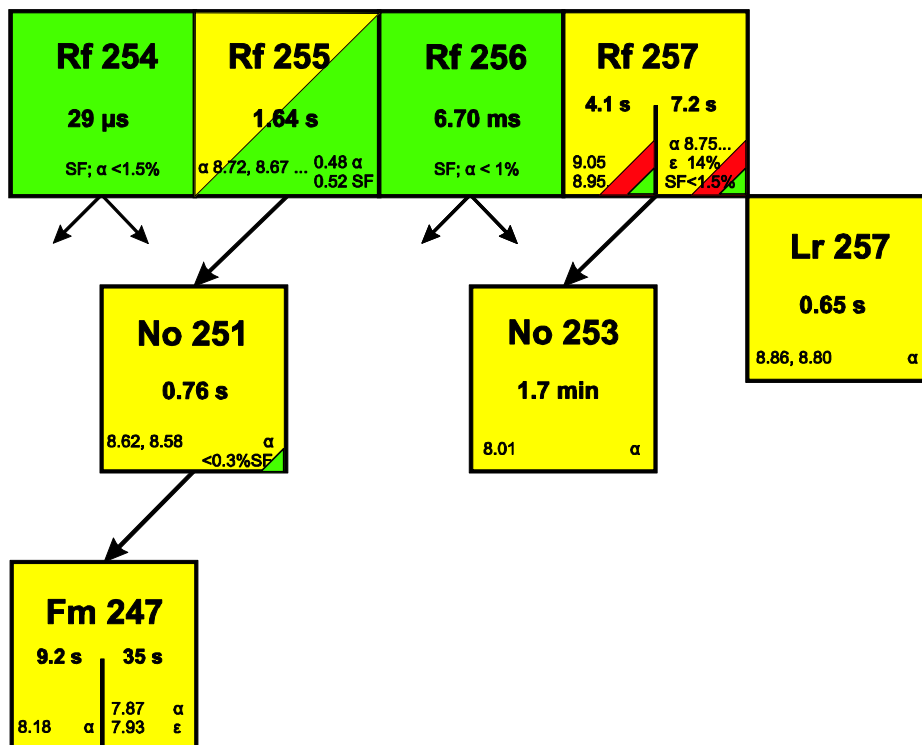


FIG 1.

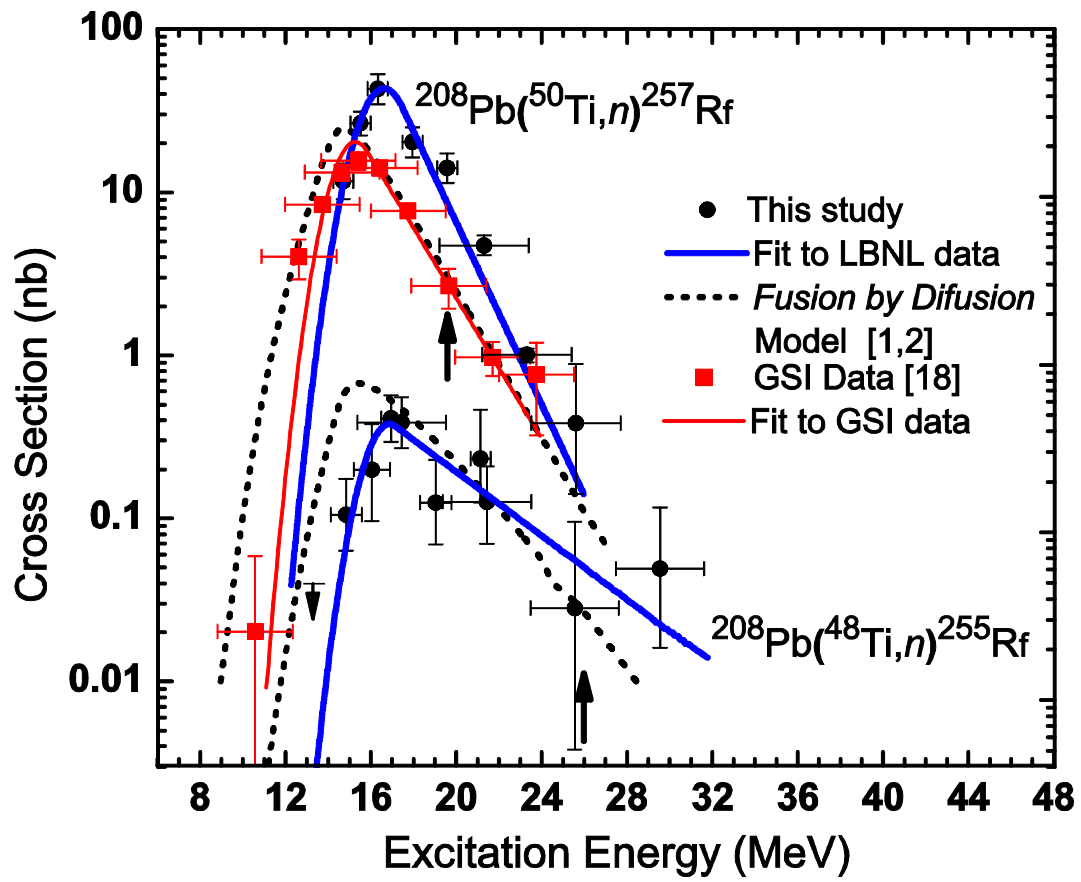


FIG 2.

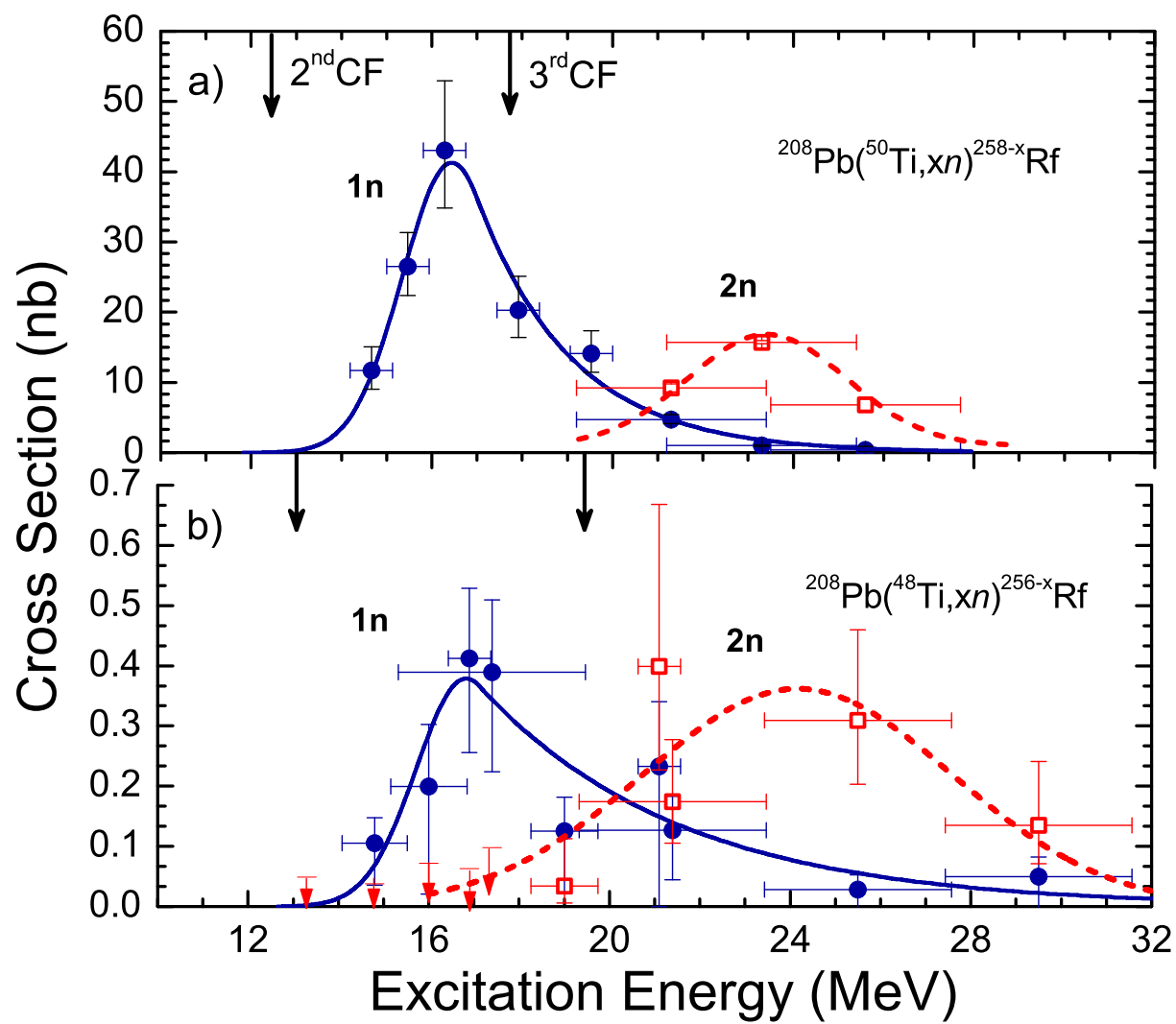


FIG 3.

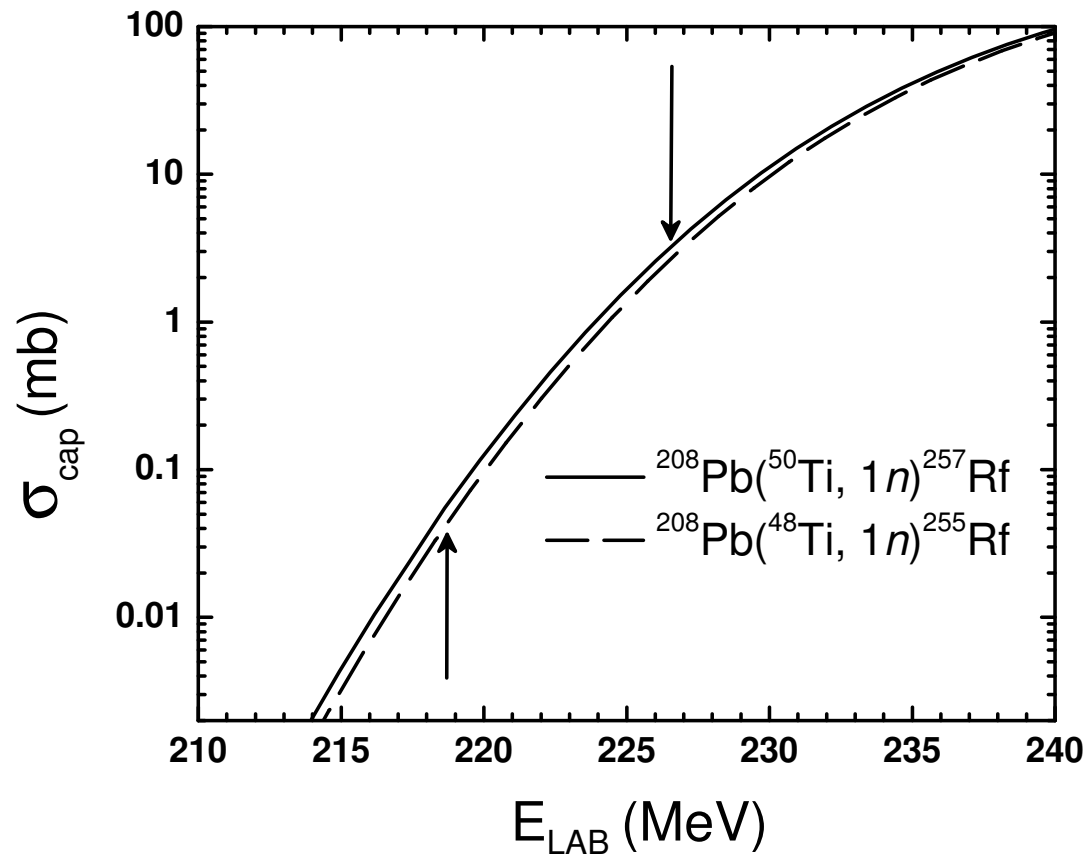


FIG 4.